

Received August 1, 2021, accepted August 11, 2021, date of publication August 20, 2021, date of current version August 31, 2021.

Digital Object Identifier 10.1109/ACCESS.2021.3106336

Dual Loop Reactive Shield Application of Wireless Power Transfer System for Leakage Magnetic Field Reduction and Efficiency Enhancement

JEDOK KIM¹ AND SEUNGYOUNG AHN¹, (Senior Member, IEEE)

The Cho Chun Shik Graduate School of Green Transportation, Korea Advanced Institute of Science and Technology (KAIST), Daejeon 34051, Republic of Korea

Corresponding author: Seungyoung Ahn (sahn@kaist.ac.kr)

This work was supported in part by the Institute of Information and Communications Technology Planning and Evaluation (IITP) funded by the Korean Government [Ministry of Science and Information and Communication Technologies (MSIT)] (Development of advanced power and signal EMC technologies for hyper-connected e-vehicle) under Grant 2020-0-00839, and in part by IITP funded by the Korean Government (MSIT) (Development of commercialization technology for ultra-small, high efficiency wireless charging for 1kW class robot) under Grant IITP-2020-0-00618.

ABSTRACT The wireless power transfer (WPT) system generates a high density leakage electromagnetic field (EMF) during its operation. Exposure to leakage EMF has adverse effects on human health. In order to reduce the leakage EMF, a shielding method can be applied to the WPT system. The shielding methods in previous studies reduced leakage EMF, but the power transfer efficiency (PTE) of the WPT system was decreased. Therefore, a shielding method providing high shielding effectiveness (SE) without PTE degradation is necessary. This paper proposes a dual loop reactive shield application for reducing leakage EMF with PTE enhancement. The proposed dual loop reactive shield generates in phase and out of phase magnetic fields simultaneously. The out of phase magnetic field depresses leakage EMF, and the in phase magnetic field increases the PTE. The proposed method is verified for the cases of symmetric and asymmetric WPT systems, including misalignment conditions. The experimental results of the symmetric WPT system showed a 2.1% PTE increase with 55.5% SE in an alignment condition, and a 3.9% PTE increase with 53% SE in a misalignment condition. In addition, the experimental results of the asymmetric WPT system presented a 1.6% PTE increase with 61.3% SE in an alignment condition, and a 2.7% PTE increase with 54.1% SE in a misalignment condition.

INDEX TERMS Wireless power transmission, electromagnetic shielding, electromagnetic compatibility, reactive shield, multi loop coil.

I. INTRODUCTION

Since an inductive power transfer system providing mid-range wireless power transfer (WPT) was introduced [1], applications of the WPT system have been drawing attention. Consumer electronics such as smartphones and smartwatches can be classified as low power WPT applications [2], [3]. On the other hand, home appliances such as televisions and unmanned aerial vehicles (UAVs) can be classified as intermediate power WPT applications. In particular, WPT applications to UAVs are gradually increasing with the proliferation of UAV applications [4]–[6].

The WPT system transmits electrical power through a magnetic field, and therefore a high density magnetic field

The associate editor coordinating the review of this manuscript and approving it for publication was Kwok L. Chung¹.

is generated during the operation. A leakage electromagnetic field (EMF) is also radiated around the WPT system, and this leakage EMF has adverse effects on human health. Furthermore, such adverse effects will increase when the power capacity of the WPT system is increased. This is because transmitting high power through the magnetic field requires greater magnetic field strength. In addition, as a human body comes into closer proximity to the WPT system, the negative influence will be increased.

For this health risk, leakage magnetic field is regulated under guidelines of international organizations such as the Institute of Electrical and Electronics Engineers (IEEE) and the International Commission on Non-Ionizing Radiation Protection (ICNIRP) [7], [8]. These guidelines are the minimum requirements for commercialization of WPT systems. However, minimizing leakage EMF is recommended for

ensuring the safety of human health even if the WPT system complies with the leakage EMF guidelines.

In order to reduce the leakage EMF, shielding such as passive shielding, active shielding, and reactive shielding can be applied [9]. Passive shielding is classified into conductive shielding and magnetic shielding. Conductive shielding reduces leakage EMF by an eddy effect [10]. The conductive shielding provides high shielding effectiveness (SE), but high heat generation and power transfer efficiency (PTE) degradation caused by the eddy effect will occur. The magnetic shielding regulates the magnetic flux path by using paramagnetic materials such as ferrite [11]. The magnetic shielding does not cause PTE degradation, but the SE is decreased when the air gap between ferrite applied to the transmitting (TX) and receiving (RX) coils is increased.

The active shielding is to eliminate the leakage EMF by generating a shielding EMF having the opposite vector direction to that of the leakage EMF. The active shielding generates a shielding EMF by its own power source, and there are two types of power supply methods: 1) dependent active shielding, and 2) independent active shielding [12]–[14]. The dependent active shielding allocates a partial shield coil having reverse winding to the TX and RX coils, respectively [12]. The TX shield coil (TS) is connected to the TX coil, and the RX shield coil (RS) is connected to the RX coil conductively. Based on this, power for the shield coils is supplied by the TX and RX coils through conductive connection, and the magnetic fields generated by shield coils have opposite vectors according to reverse winding. As a result, the shielding EMF generated by the shield coil causes magnetic cancellation, and therefore the leakage EMF is decreased. However, dependent active shielding causes degradation of PTE because of the decreased mutual inductance between the TX and RX coils.

Independent active shielding supplies shielding power from an independent power source [13], [14]. This method can appropriately control the shielding current in terms of the current strength and phase. Unlike the dependent active shielding, independent active shielding has lower PTE degradation than dependent active shielding. This is because the shield coil of independent active shielding is not conductively connected with the TX and RX coils, and consequently the coupling coefficient between the TX and RX coils is not decreased. However, independent active shielding requires an additional power source to supply power to the shield coil. For this reason, cost of the shielding application is higher than that of the other types of shielding.

Reactive shielding is another way to reduce a leakage EMF [15]–[17]. The operation principle of the reactive shield is similar to that of the active shield, but the method of supplying power to the shield coil is different. The reactive shield generates shielding EMF by leakage EMF. When the leakage magnetic field is excited to the reactive shield, the induced voltage is generated at the shield coil. The reactive shield generates shielding EMF by this induced voltage. This means that a reactive shield can operate

like active shielding without a conductive connection or additional power source. This prevents the decrease of the coupling coefficient of the TX and RX coils, and hence the PTE is decreased less compared with the dependent active shielding. In addition, an independent power source is not required, and therefore the cost of shielding application is lower than that of independent active shielding. On the other hand, the SE of reactive shielding is similar to that of active shielding. This is because reactive shielding operates based on magnetic cancellation, as in the case of active shielding.

However, the reactive shield in previous studies could not prevent the decrease of PTE, similar to active shielding. In addition, as the SE is increased, PTE accordingly decreases. In other words, a high SE causes high PTE degradation, and low PTE degradation decreases the SE. This tradeoff between PTE and SE limits reactive shield application. Therefore, a new reactive shielding preventing decreased PTE of the WPT system is necessary.

This paper proposes a new reactive shielding method having SE with increased PTE. The proposed shielding method utilizes a dual loop shield coil, and the dual loop reactive coil generates out of phase and in phase magnetic fields simultaneously. The out of phase magnetic field depresses leakage EMF, and the in phase magnetic field enhances the PTE. Based on this operation, leakage EMF is reduced and PTE is enhanced. This paper is organized as follows. In Section II, the operation principle of the proposed shielding is described. In Section III, the PTE enhancement method using the shield coil is described. In Section IV, experimental verifications of the proposed shielding method in terms of the SE and PTE are presented.

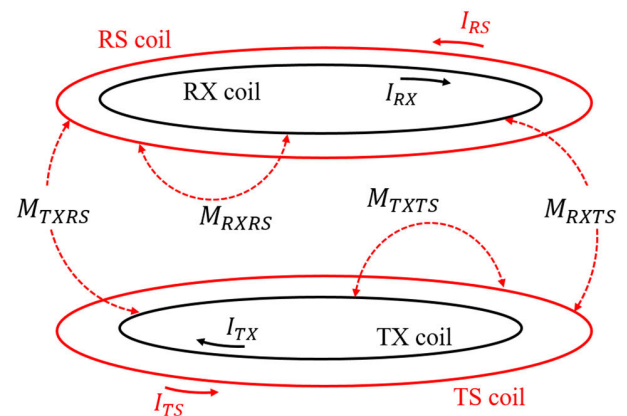


FIGURE 1. Mutual inductance between TX, RX and shield coil.

II. OPERATION PRINCIPLE OF DUAL LOOP REACTIVE SHIELD

A. PREVIOUS REACTIVE SHIELD OVERVIEW

Figure 1 shows the mutual inductance between the TX, RX, and shield coils of the WPT system with application of the previous reactive shield. The TS and RS shield coils applied to the TX and RX coils have mutual inductance with the TX

and RX coils for supplying power, and mutual inductances are defined as (1). Note that iX is the arbitrary TX or RX and iS is the arbitrary TS or RS. k_{iXiS} is the coupling coefficient between iX and iS coil, and L is the inductance.

$$M_{iXiS} = k_{iXiS} \sqrt{L_{iX} L_{iS}} \quad (1)$$

The resonant frequency of the reactive shield is tuned to have inductive reactance for the operating frequency by adjusting the capacitance. In this case, the previous reactive shield generates out of phase EMF for the TX and RX coils. While the WPT operation, the TX and RX inductances L_{TX} and L_{RX} are influenced by M_{iXiS} . The TS and RS coils have out of phase current for the TX and RX coil current, and therefore the effective inductance $L_{iX-effective}$ including M_{iXiS} can be calculated as (2). The decrease of $L_{iX-effective}$ caused by the M_{iXiS} decreases the quality factor of the TX and RX coils, as given in (3). The decrease of $Q_{iX-loaded}$ of TX and RX coils increases the energy loss because energy that can be stored in the coil will decrease. As a result, the PTE of the WPT system will decrease because the quality factor decreases when the previous reactive shield is applied. This means that PTE decrease can be prevented by preserving the quality factor of the WPT coil, and furthermore the PTE can be enhanced if the quality factor of the WPT can be increased.

$$L_{iX-effective} = L_{iX} - \sum M_{iXiS} \left(\frac{I_{iS}}{I_{iX}} \right) \quad (2)$$

$$Q_{iX-loaded} = \frac{\omega_0 \left(L_{iX} - \sum M_{iXiS} \left(\frac{I_{iS}}{I_{iX}} \right) \right)}{R_{iX}} \quad (3)$$

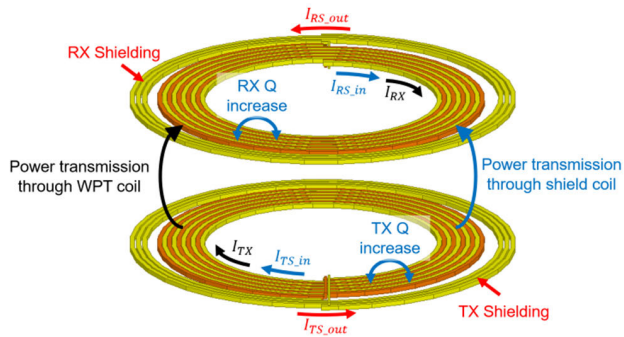


FIGURE 2. Concept of proposed dual loop reactive shield.

B. PROPOSED DUAL LOOP REACTIVE SHIELD

1) OPERATION PRINCIPLE AND ADVANTAGES

Figure 2 shows the concept of the proposed dual loop reactive shield. The proposed TS and RS coils have an inner and outer loop, respectively, and the inner and outer loops are connected to each other. The inner loop coil generates an in phase EMF and the outer loop coil generates an out of phase EMF for the TX and RX coils. In this case, the decrease of the quality factor of the TX and RX coils caused by the outer loop of the TS and RS coils can be compensated by the inner loop of the TS and RS coils. Based on these two loop operations,

PTE degradation by the decrease of the quality factor can be prevented.

The proposed reactive shield has advantages compared with the previous reactive shield in terms of the SE, PTE, and volume [15]–[17]. The reactive shielding method in [15] utilizes a shield coil having a small radius, and the position of the shield coil is far from the WPT system. In this case, the decrease of the PTE by the shield coil is reduced, but leakage EMF in the surrounding area of the WPT system cannot be reduced. In addition, the position of the reactive shield is far from the WPT system, and therefore reactive shield cannot be included in the WPT system. Likewise, the reactive shielding method in [16] utilizes a shield coil having a small radius, and the shield coil position is far from the WPT system. In addition, the shield coil in [16] requires a conductive connection between powering and the shield coil. Consequently, the requirement of the shielding application is higher than that of the reactive shield in [15].

The approach in [17] is a reactive shield for a wireless smartphone charger, and it provides SE for the surrounding area of the WPT system. In addition, the shield coil can be applied in a WPT system as one module. However, the method in [17] cannot avoid a decrease of PTE because the effective inductance of the coil is decreased due to the negative mutual inductance by the shield coil. The wireless smartphone charger is a low power WPT system, and therefore the actual electrical loss might not be high. However, the actual electrical loss may be increased when the power capacity of the WPT system is increased. For this reason, the method in [17] has limited application to high power WPT systems.

On the contrary to this, the proposed method does not decrease the PTE, and it provides SE for the surrounding area of the WPT system. In addition, the number of coil turns including iX and inner iS is identical to that the WPT system without (w/o) a shield. Moreover, the inner and outer shield coil are connected, and thus the required capacitor is identical to that in [17]. For this reason, the proposed method has no additional material requirement compared with the method in [17]. Therefore, the proposed reactive shield has advantages relative to [17] in terms of the PTE.

2) INDUCTANCE AND COUPLING COEFFICIENT

The inductance calculation for multi-structure coil has been researched in [18]. The total inductance of a multi-structure coil is calculated by the sum of the inductance according to the total length of the coil and the mutual inductance between turns. Based on this calculation, the simplified inductance calculation of the proposed dual loop coil can be calculated as (4). Note that $L_{iS-self}$ is the self-inductance of dual loop coil, and $L_{in-self}$ and $L_{out-self}$ are the self-inductances of the inner and outer loop. M_{in-out} is the mutual inductance between the inner and outer loop.

$$L_{iS-self} = L_{in-self} + L_{out-self} - M_{in-out} \quad (4)$$

The coupling coefficient between two coils is defined as the magnetic flux linkage of total coil turns [19]. In the case of dual loop coils, the outer loop has reverse winding for the inner loop. This means that the outer loop coil has a negative coupling coefficient for the coupling coefficient between the iX coil and inner loop coil. In this case, the coupling coefficient between the iX and iS coils can be calculated as (5). In order to operate the proposed shielding, k_{iXiSin} should be larger than $k_{iXiSout}$ ($k_{iXiSin} > k_{iXiSout}$). This is because the outer loop coil will have in phase current when $k_{iXiSout}$ is larger than k_{iXiSin} . In this case, leakage EMF around the WPT system will increase.

In addition, there are four coupling coefficients between the TS and RS coils: coupling between the inner loop k_{in} , coupling between the outer loop k_{out} , and two couplings between the inner and outer loop k_{in-out} . Based on this, the coupling coefficient between dual loop coils can be calculated as (6). k_{in-out} decreases k_{TSRS} , and therefore minimizing the number of outer loop coil turns is beneficial for maintaining PTE.

$$k_{iXiS} = k_{iXiSin} - k_{iXiSout} \tag{5}$$

$$k_{TSRS} = \frac{k_{in} + k_{out}}{2} - k_{in-out} \tag{6}$$

3) CAPACITANCE SELECTION

The TS coil is adjacent to the TX coil, and the RS coil is adjacent to the RX coil, and consequently k_{TXTS} and k_{RXRS} are strong. This strong coupling coefficient causes frequency splitting. Figure 3 shows the frequency splitting and zero phase angle. Frequency splitting decreases the power transfer capacity (PTC) in resonant frequency ω_0 defined by the coil self-inductance, and therefore a WPT system tuned as ω_0 cannot be used. In this case, new resonant frequency should be determined, including a strong coupling coefficient [20], [21].

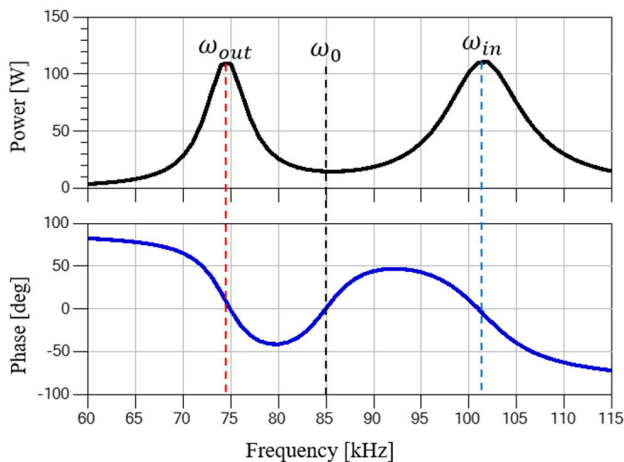


FIGURE 3. Frequency splitting and zero phase angle.

In Figure 3, there are two additional zero phase angle frequencies, defined as the out of phase resonant frequency

ω_{out} and in phase resonant frequency ω_{in} . ω_{out} makes the current of adjacent two coils to be an out of phase. This means that the two coils generate an EMF having an opposite vector direction. If two coils have a strong coupling coefficient, the PTE will significantly decrease because of the decrease of the quality factor caused by the negative magnetic field effect.

On the other hand, ω_{in} makes the current of adjacent two coils to be in phase. In this case, two coils generate an EMF having forward direction. If two coils are tuned to ω_{in} with a strong coupling coefficient, two separated coils can be regarded as a single coil [21]. Therefore, the resonant frequency of two coils having a strong coupling condition should be tuned to ω_{in} . The capacitances of iX and iS for ω_{in} C_{iX-in} and C_{iS-in} are calculated as (7) and (8) [20].

$$C_{iX-in} = \frac{1}{\left(2\pi \left(\sqrt{1 + k_{iXiS} \left(\sqrt{\frac{L_{iS}}{L_{iX}}}\right)}\right) f_0\right)^2 \times L_{iX}} \tag{7}$$

$$C_{iS-in} = \frac{1}{\left(2\pi \left(\sqrt{1 + k_{iXiS} \left(\sqrt{\frac{L_{iX}}{L_{iS}}}\right)}\right) f_0\right)^2 \times L_{iS}} \tag{8}$$

Since the iX and iS coils are tuned as ω_{in} , the TX and TS coils generate an in phase EMF for each other. In addition, the RX and RS coils generate an in phase EMF for each other. However, TX and TS have phase difference for the RX and RS magnetic fields because C_{iX-in} and C_{iS-in} do not include the coupling coefficient across the coils. Therefore, a WPT system tuned to ω_{in} can operate like a conventional two coil WPT system.

The outer loop of the shield coil has reverse winding with the inner loop, and therefore shielding EMF is generated. The outer loop of TS coil generates shielding effect for the leakage EMF generated from the TX and TS inner loops. Likewise, the outer loop of the RS coil generates shielding EMF for the leakage EMF generated from the RX and RS inner loops. Based on this operation, leakage EMF around the WPT system is reduced.

C. SHIELDING EFFECTIVENESS CALCULATION

Figure 4 shows the geometrical array of the TX, RX, TS, and RS coils, and the distance to point p from the center of each coil. The EMF at point p is determined according to the coil radius, current strength, and distance between the coil center and point p . In the case of the proposed shielding, the coils having multiple turns are utilized. In this case, the total magnetic flux density of each coil loop can be calculated by the summation of the magnetic flux density generated from each turn as (9). t ($t = 1, 2, \dots, n$) is each coil turn.

$$B_{loop} \approx \sum_{t=1}^n \oint B_t \cdot dl \tag{9}$$

The radius of each coil turn is gradually changed as much as the coil diameter and the space between each turn. This variation causes variation of the EMF at point p . By reflecting

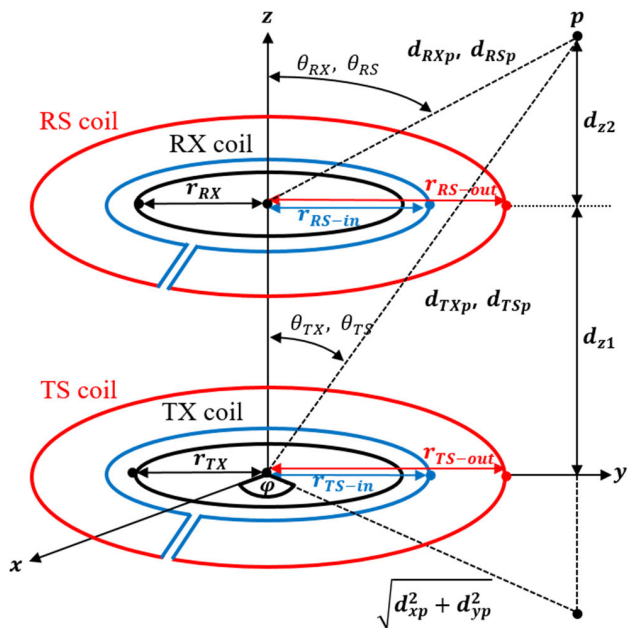


FIGURE 4. Geometrical coil array and distance to point p of a proposed shield coil applied WPT system.

this coil radius variation, the EMF at point p B_{p-loop} can be calculated as (10-1). Note that μ_0 is the permeability of free space, k_0 is the wave number ($2\pi/\lambda$), λ is the wavelength (c/f), c is the velocity of light (3×10^8 m/s), f is the frequency, and r_t is the coil radius of t turn. d_{p-t} is the distance between the coil center and point p , and the distance for the TX and TS coils is calculated as (11), and the distance for RX and RS is calculated as (12).

$$B_{p-loop} = AB - CD \quad (10)$$

$$A = \sum_{t=1}^n j\mu_0 \frac{k_0 r_t^2 I_0 \cos \theta_{p-t}}{2d_{p-t}^2} \quad (10-1)$$

$$B = \left[1 + \frac{1}{jk_0 d_{p-t}} \right] e^{-jk_0 d_{p-t}} \cdot \vartheta_t \quad (10-2)$$

$$C = \sum_{t=1}^n \mu_0 \frac{(k_0 r_t)^2 I_0 \sin \theta_{p-t}}{4d_{p-t}} \quad (10-3)$$

$$D = \left[1 + \frac{1}{jk_0 d_{p-t}} - \frac{1}{(k_0 r_t)^2} \right] e^{-jk_0 d_{p-t}} \cdot \vartheta_t \quad (10-4)$$

where $\vartheta_t = \sin \theta_{p-t} \cos \varphi_{p-t} \cos \theta_{p-t}$

$$d_{TXp}, d_{TSsp} = \sqrt{\left(\sqrt{d_{xp}^2 + d_{yp}^2}\right)^2 + (d_{z1} + d_{z2})^2} \quad (11)$$

$$d_{RXp}, d_{RSsp} = \sqrt{\left(\sqrt{d_{xp}^2 + d_{yp}^2}\right)^2 + d_{z2}^2} \quad (12)$$

Figure 5 shows the phasor diagram of the magnetic fields at point p generated by the proposed shielding. TX and RX generate B_{pTX} and B_{pRX} , and inner TS and RS generate B_{pTSin} and B_{pRSin} . These magnetic fields are in phase relative to each other, and the total leakage EMF at point p $B_{pl-total}$ can be calculated by vector summation of the in phase magnetic field according to (14) assuming that they are ideally in phase.

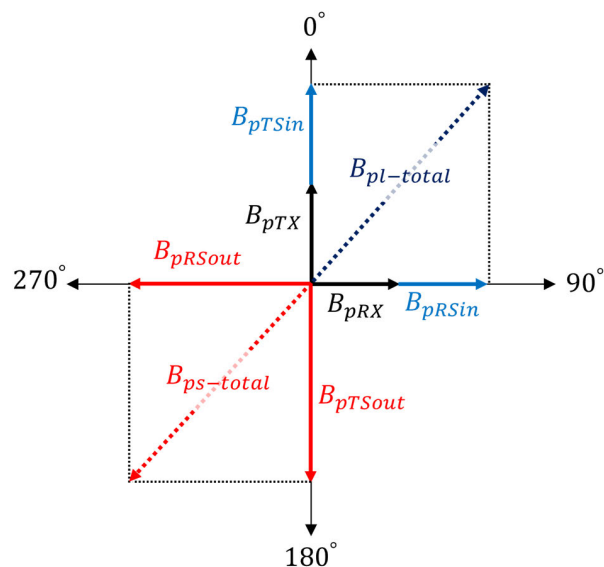


FIGURE 5. Phasor diagram of a proposed shield coil applied WPT system.

Note that ϑ_{iX} and ϑ_{iSin} are the current phases of the iX and iS coils.

$$B_{p-iXiSin} = (B_{piX} + B_{piSin}) \cos \left(\frac{\vartheta_{iX} - \vartheta_{iSin}}{2} \right) \quad (13)$$

$$B_{pl-total} = (B_{p-TXTSin} + B_{p-RXRSin}) \cos \left(\frac{\vartheta_{TXTSin} - \vartheta_{RXRSin}}{2} \right) \quad (14)$$

where, $\vartheta_{TXTSin} = \vartheta_{TX} = \vartheta_{TSin}$, $\vartheta_{RXRSin} = \vartheta_{RX} = \vartheta_{RSin}$

The magnetic fields generated from the outer loop of the shield coils will be the shielding EMF. B_{pTSout} reduces B_{pTX} and B_{pTSin} , and B_{pRSout} reduces B_{pRX} and B_{pRSin} respectively. The total shielding EMF $B_{ps-total}$ is calculated using (15), and the phase of the shielding EMF is calculated with (16). The condition having maximum SE is that $B_{pl-total}$ and $B_{ps-total}$ have identical magnitude with a 180° phase difference.

$$B_{ps-total} = (B_{pTSout} + B_{pRSout}) \cos \left(\frac{\vartheta_{TSout} - \vartheta_{RSout}}{2} \right) \quad (15)$$

$$\vartheta_{ps-total} = \left\{ \tan^{-1} \left(\frac{B_{pRSout}}{B_{pTSout}} \right) - \frac{90 - (\vartheta_{TSout} - \vartheta_{RSout})}{2} \right\} - 180 \quad (16)$$

where $0^\circ \leq \vartheta_{TSout} - \vartheta_{RSout} \leq 90^\circ$

The total EMF $B_{p-total}$ of the proposed shield coil applied to a WPT system is calculated as (17). Obviously, the SE may be enhanced when $B_{p-total}$ is minimized. In order to achieve a high SE, $B_{ps-total}$ should be identical to $B_{pl-total}$ with 180° phase difference. As a result, the SE of the proposed shielding at point p is determined as (18). In addition, the SE for other WPT systems such as a conventional two coil WPT system or other shielding is estimated by the ratio of the total EMF of the proposed system $B_{p-proposed}$ and the total EMF of the comparison target system $B_{p-target}$ as delineated in (19).

$$B_{p-total} = B_{pTX} + B_{pRX} + B_{pTSin} + B_{pRSin} + B_{pTSout} + B_{pRSout} \quad (17)$$

$$SE_p = \left(1 - \frac{B_{p-total}}{B_{pTX} + B_{pRX} + B_{pTSin} + B_{pRSin}}\right) \times 100 \quad (18)$$

$$SE_{p-compare} = \left(1 - \frac{B_{p-proposed}}{B_{p-target}}\right) \times 100 \quad (19)$$

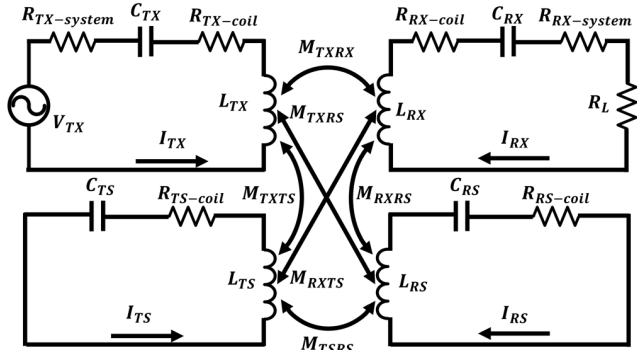


FIGURE 6. Equivalent circuit model of WPT system applied proposed shield coil.

III. PTE ENHANCEMENT OF PROPOSED SHIELDING

A. CIRCUIT ANALYSIS

Figure 6 shows the equivalent circuit model of WPT system with application of the shield coil. The multi-coil applications for increasing the PTE were studied in terms of the impedance variation [20]–[24]. For the proposed shielding method, Kirchhoff’s voltage law (KVL) for the equivalent circuit can be expressed as

$$\begin{aligned} & \frac{V_{TX}}{j\omega L_{TX} I_{TX}} \\ &= \left(\frac{R_{TX}}{j\omega L_{TX} I_{TX}} + 1 - \frac{\omega_0^2}{\omega_{TX}^2} \right) + k_{TXRX}^2 L_{RX} \left(\frac{I_{RX}}{I_{TX}} \right) \\ & \quad + k_{TXTS}^2 L_{TS} \left(\frac{I_{TS}}{I_{TX}} \right) + k_{TXRS}^2 L_{RS} \left(\frac{I_{RS}}{I_{TX}} \right) \quad (20-1) \end{aligned}$$

$$\begin{aligned} 0 &= \left(\frac{R_{TS}}{j\omega L_{TS} I_{TS}} + 1 - \frac{\omega_0^2}{\omega_{TS}^2} \right) + k_{TXTS}^2 L_{TX} \left(\frac{I_{TX}}{I_{TS}} \right) \\ & \quad + k_{RXTS}^2 L_{RX} \left(\frac{I_{RX}}{I_{TS}} \right) + k_{TSRS}^2 L_{RS} \left(\frac{I_{RS}}{I_{TS}} \right) \quad (20-2) \end{aligned}$$

$$\begin{aligned} 0 &= \left(\frac{R_{RS}}{j\omega L_{RS} I_{RS}} + 1 - \frac{\omega_0^2}{\omega_{RS}^2} \right) + k_{TXRS}^2 L_{TX} \left(\frac{I_{TX}}{I_{RS}} \right) \\ & \quad + k_{RXRS}^2 L_{RX} \left(\frac{I_{RX}}{I_{RS}} \right) + k_{TSRS}^2 L_{TS} \left(\frac{I_{TS}}{I_{RS}} \right) \quad (20-3) \end{aligned}$$

$$\begin{aligned} 0 &= \left(\frac{R_{RX}}{j\omega L_{RX} I_{RX}} + 1 - \frac{\omega_0^2}{\omega_{RX}^2} \right) + k_{TXRX}^2 L_{TX} \left(\frac{I_{TX}}{I_{RX}} \right) \\ & \quad + k_{RXTS}^2 L_{TS} \left(\frac{I_{TS}}{I_{RX}} \right) + k_{RXRS}^2 L_{RS} \left(\frac{I_{RS}}{I_{RX}} \right) \quad (20-4) \end{aligned}$$

Note that V_{TX} is the input voltage of the TX and shielding coil and I is the current. R , L , and C are the resistance, inductance, and capacitance, respectively. ω_0 is the operating frequency ($2\pi f$), and ω_{iX} and ω_{iS} are the actual resonant

frequency of the iX and iS coils defined as $1/\sqrt{LC}$. R_L is the load resistance. From the KVL equation, the reflected inductance from the TS and RS coils is $k_{iXIS}^2 L_{iS} (I_{iS}/I_{iX})$.

Since the resonant frequency of the WPT system, including the TS and RS coils, is tuned to be in phase, the reflected inductance is added to the effective inductance. In this case, the effective inductance of the iX and iS coils including k_{TXTS} and k_{RXRS} can be calculated as (21) and (22), except for the other mutual inductance. Based on the effective inductance, the loaded quality factor of iX coil $Q_{iX-loaded}$ and the loaded quality factor of iS coil $Q_{iS-loaded}$ can be calculated as (23) and (24). Note that R_{TX} is the sum of $R_{TX-system}$ and $R_{TX-coil}$, and R_{RX} is the sum of $R_{RX-system}$, $R_{RX-coil}$, and R_L .

$$L_{iX-effective} = L_{iX} + k_{iXIS}^2 L_{iS} \left(\frac{I_{iS}}{I_{iX}} \right) \quad (21)$$

$$L_{iS-effective} = L_{iS} + k_{iXIS}^2 L_{iX} \left(\frac{I_{iX}}{I_{iS}} \right) \quad (22)$$

$$Q_{iX-loaded} = \frac{\omega_{in} \left(L_{iX} + k_{iXIS}^2 L_{iS} \left(\frac{I_{iS}}{I_{iX}} \right) \right)}{R_{iX}} \quad (23)$$

$$Q_{iS-loaded} = \frac{\omega_{in} \left(L_{iS} + k_{iXIS}^2 L_{iX} \left(\frac{I_{iX}}{I_{iS}} \right) \right)}{R_{iS}} \quad (24)$$

B. Q-BOOSTED POWER TRANSMISSION

Since the TX and RX coils are connected with the system, they have lower quality factors than the TS and RS coils. This is because the quality factor of the TX and RX coils is calculated including the system resistance. If the quality factor of the TX and RX coils remains low, the PTE cannot be increased. This is because all power transmission channels of the WPT system include TX and RX coils. In order to increase the quality factor of these coils, quality factor boosting according to the reflected inductance can be used. The reflected inductance of the TX and RX coils is determined by the coupling coefficient, the current ratio with the shield coil, and the inductance of the shield coil as given in (21). Coupling coefficient control requires changes of the coil position or inner and outer coil design. Likewise, changes of the shield coil inductance require changes to coil design. Therefore, these two parameters cannot be tuned. However, the current ratio between two coils is controllable. In the KVL equation, ω_0^2/ω_{iX}^2 and ω_0^2/ω_{iS}^2 cause impedance variation, and this can be controlled by tuning capacitance.

Since the WPT system, including the shield coil, is tuned to in phase resonant frequency, the resonant condition of the WPT system includes the reflected inductance of the shield coil, as in (7) and (8). However, this reflected inductance is changed in a loaded condition, as given in (21) and (22). This means that the resonant condition of the WPT system is changed according to the changes of I_{iX} and I_{iS} . Concretely, the amount of current variation corresponds to the amount of capacitance variation because the other parameters are not changed. In addition, $L_{iX-effective}$ is changed as much

as the variation of the current magnitude of iX and iS coil. This means that the amount of the resonant condition change by capacitance variation corresponds to the amount of the $L_{iX-effective}$ variation symmetrically. Based on this characteristic of the resonant condition changes, capacitance tuning for the iX and iS can be generalized as (25) and (26) for an increase of $Q_{iX-loaded}$.

$$C_{iX-boost} = \frac{1}{(2\pi f_0)^2 \times L_{iX-effective}} - C_{tuning} \quad (25)$$

$$C_{iS-boost} = \frac{1}{(2\pi f_0)^2 \times L_{iS-effective}} + C_{tuning} \quad (26)$$

where $C_{iS-in} < C_{iS-boost} < C_{\omega_0}$

The capacitance tuning according to (25) and (26) has two implications in terms of the PTE. One is the increase of power transmission through shield coil, and the other is an increase of $Q_{iX-loaded}$. Firstly, the increase of power transmission through the shield is beneficial for the PTE because $Q_{iS-loaded}$ is much higher than $Q_{iX-loaded}$. This means that the ratio of high quality factor based power transmission is increased. This can be described in terms of the induced voltage of the RX coil defined as (27) and the resistance. Reduced I_{TX} causes a reduction of TX loss, defined as $I_{TX}^2 R_{TX}$, but transferred power to the RX coil is decreased in proportion to the decrease of I_{TX} . However, I_{TS} has increased and therefore the induced voltage to the RX coil is compensated by the increase of $j\omega M_{RXTS} I_{TS}$ and $j\omega M_{RXRS} I_{RS}$. R_{iS} is lower than R_{iX} ($R_{iX} = R_{iX-coil} + R_{iX-system}$), and thus power is transmitted with reduced loss. However, the decrease of PTC is inevitable because shield coils induce loss of $I_{iS}^2 R_{iS}$. In other words, PTC is decreased as much as the amount of $I_{TS}^2 R_{TS}$ and $I_{RS}^2 R_{RS}$.

$$V_{RX} = j\omega M_{TXRX} I_{TX} + j\omega M_{RXTS} I_{TS} + j\omega M_{RXRS} I_{RS} \quad (27)$$

On the one hand, the increase of $Q_{iX-loaded}$ leads to enhanced PTE. The TX and RX coils are the start and end for all power transmission channels. This means that the PTE for all transmission channels will increase when $Q_{iX-loaded}$ is increased. Based on this quality factor boosting, the proposed shield can enhance PTE during the shielding operation.

Critical coupling is the condition to transfer maximum power, and the critical coupling of the proposed system is calculated as (28). The increase of the quality factor causes changes to the critical coupling condition. If the coupling coefficient between two coils is lower than the critical coupling, that condition is defined as under coupling ($k_{coils} < k_{critical}$). When the WPT system operates in under coupling conditions, PTC and PTE will decrease.

$$k_{critical} = \frac{1}{\sqrt{(\sqrt{Q_{TX} Q_{TS}}) (\sqrt{Q_{RX} Q_{RS}})}} \quad (28)$$

On the other hand, when the coupling coefficient between two coils is higher than the critical coupling, that condition is defined as over coupling ($k_{coils} > k_{critical}$). When the WPT system operates in an over coupling condition, PTC

is decreased, but PTE is increased, unlike the case of under coupling. For this reason, the WPT system can be designed to have over coupling conditions. However, excessive inductance allocation causes the PTC to decrease significantly. Therefore, an over coupling condition is determined in terms of the tradeoff between PTE and PTC.

Based on these characteristics, PTE η including the power consumption of the shield coil is calculated as (29). In order to enhance the PTE, the power consumption caused by the system and coil resistance should be minimized. The proposed system is designed to have higher I_{TS} and I_{RS} than I_{TX} and I_{RX} for quality factor boosting. As a result, the boundary condition of the PTE enhancement can be considered in terms of the loss variation of each coil. The condition of PTE enhancement is that the power loss in the boosted condition should be lower than the power loss in the non-boosted condition, as delineated in (30). Note that P_{TX} , P_{TS} , and P_{RS} are the power loss of TX, TS, and RS in the non-boosted condition, and P_{TX-b} , P_{TS-b} , and P_{RS-b} are the power loss of TX, TS, and RS in the boosted condition.

$$\eta = \frac{R_L |I_{RX}|^2}{R_{TX} |I_{TX}|^2 + (R_{RX} + R_L) |I_{RX}|^2 + R_{TS} |I_{TS}|^2 + R_{RS} |I_{RS}|^2} \quad (29)$$

$$P_{TX} + P_{TS} + P_{RS} < P_{TX-b} + P_{TS-b} + P_{RS-b} \quad (30)$$

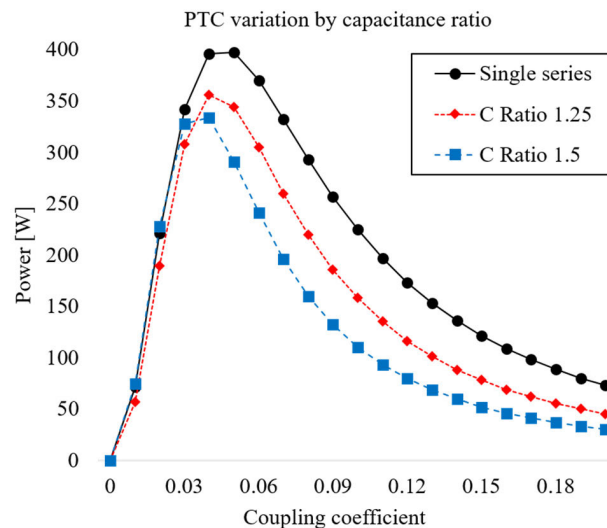


FIGURE 7. PTC variation according to capacitance ratio.

Figure 7 shows the PTC variation according to the capacitance ratio. The capacitance ratio results in current variation, and the current variation causes quality factor variation. The critical coupling is shifted to a lower coupling coefficient with an increase of the quality factor. The more the capacitance ratio is increased, the more PTC is decreased. The decrease of PTC can be analyzed in terms of the increased quality factor and power losses of TS and RS coil. First, the critical coupling condition is the impedance

matching condition, defined as $Z_{TX} = Z_{RX}$, and therefore maximum power is transmitted in critical coupling. This means that the increase of over coupling results in an increase of impedance mismatching between TX and RX coil. For this reason, PTE will decrease as much as the increase of over coupling. The other reason is the increase of the power consumption in TS and RS coils ($I_{iS}^2 R_{iS}$).

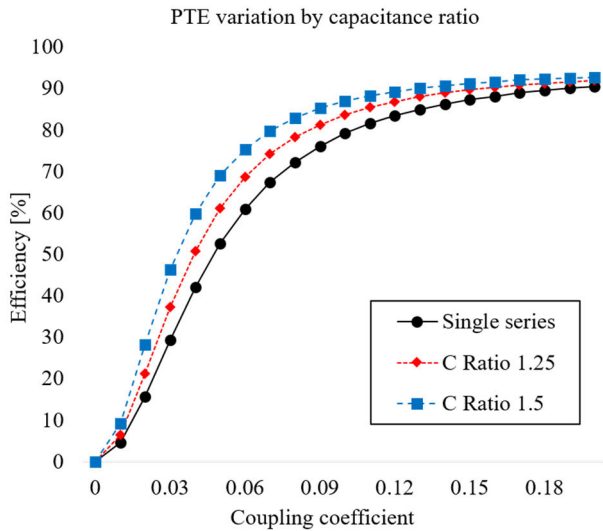


FIGURE 8. PTE variation according to capacitance ratio.

Figure 8 shows the PTE variation according to the capacitance ratio. The increase of PTE can be explained in terms of the power transmission through a shield coil having a high quality factor, and the increase of the TX and RX quality factor. In addition, the proposed shielding method is beneficial for maintaining the PTE in a misalignment condition. The misalignment of the TX and RX coils decreases the coupling coefficient between these coils. In this case, PTE decreases as much as the coupling coefficient decreases. However, the amount of the PTE decrease differs in accordance with the quality factor. When the WPT system operates with a high quality factor, the decrease of PTE according to the decrease of the coupling coefficient is reduced. This means that the proposed shielding method has advantages not only of increasing the PTE in an alignment condition, but also of maintaining the PTE in a misalignment condition.

C. DETERMINATION OF OUTER LOOP TURNS

Figure 9 shows the mutual inductance variation in accordance with the number of outer loop turns. The outer loop of the shield coil has reverse winding with the inner loop of the shield coil, and the total coupling coefficient between coils is determined by the sum of inner and outer loop coupling coefficient defined as (5) and (6). As a result, the increase of the outer loop turns decreases the mutual inductance with the iX coil.

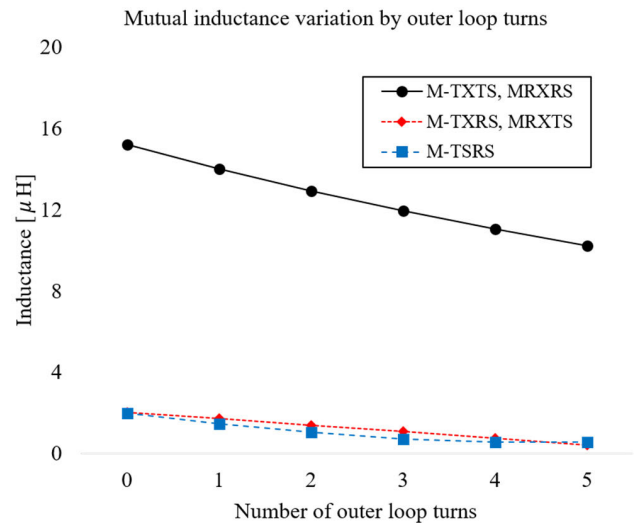


FIGURE 9. Mutual inductance variation in accordance with the number of outer loop turns.

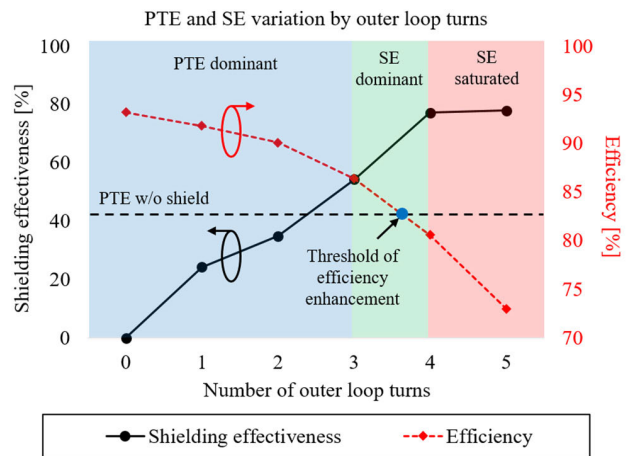


FIGURE 10. PTE and SE variation in accordance with the number of outer loop turns.

The decrease of M_{TXTS} and M_{RXRS} reduces the quality factor boosting effect. This means that the effective inductance of the TX and RX coils cannot be effectively increased at an identical current ratio. In addition, decreases of M_{TXRS} , M_{RXTS} , and M_{TSRS} reduce the power transmission through the shield coil.

Figure 10 shows the PTE and SE variation in accordance with the number of outer loop turns. The decrease of PTE is increased in proportion to the increase of outer loop turns. This is because the increase of the number of outer loop turns decreases the TX and RX quality factors as well as M_{TXRS} , M_{RXTS} , and M_{TSRS} .

The characteristics of the PTE and SE can be classified according to 1) a PTE dominant region, 2) a SE dominant region, and 3) a SE saturated region. The PTE dominant region is the region where the PTE of the WPT system

increases compared with the case without (w/o) shield. In this case, PTE is increased with low SE. The PTE dominant region has a different characteristic with the other previous shielding methods. The previous shielding methods sought a tradeoff between a decreased PTE and increased SE. This means that a small PTE decrease causes low SE. In other words, previous shielding methods could not contribute to PTE enhancement even if the SE is low. On the other hand, the proposed shielding method seeks a tradeoff between increased PTE and decreased SE. If the WPT system requires a low SE, the function of the proposed method can be allocated to PTE enhancement, unlike the previous shielding methods.

The SE dominant region is the region where high SE occurs with a decrease of PTE. Although the PTE is decreased in the SE dominant region, the amount of the PTE decrease is less than that of other previous shielding method with an identical SE. This region can be utilized when the WPT system requires a high SE. The SE saturated region is the region where $B_{ps-total}$ is stronger than $B_{pl-total}$. In this case, $B_{ps-total}$ will be a leakage EMF and hence the SE will decrease in proportion to the increase of the outer loop turns. In addition, the decrease of PTE is increased in proportion to the increase of outer loop turns. Therefore, the SE dominant region will be a boundary determining the number of outer loop turns.

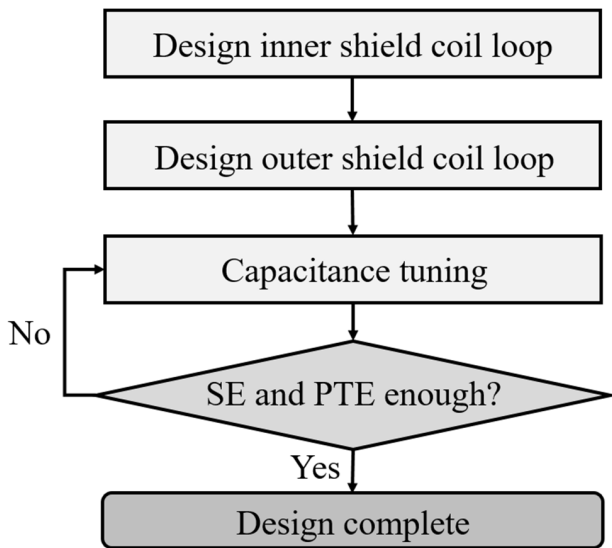


FIGURE 11. Design flow of proposed reactive shield.

D. DESIGN STRATEGY OF A PROPOSED SHIELD

Figure 11 shows the design flow of the proposed reactive shield. The design process of the proposed reactive shield is segmented into four steps as follows: 1) inner shield coil design, 2) outer shield coil design, 3) capacitance tuning, and 4) SE and PTE evaluation. A key element of inner shield coil design is to have a high coupling coefficient with the adjacent iX coil ($k_{TXTS} \cong k_{RXRS} \cong 1$). In order to have a high coupling coefficient, it is recommended to design an inner shield coil

loop having an identical radius and turns with the adjacent iX coil.

The design criteria of the outer shield coil loop can differ according to the target SE and PTE described in Figure 10. However, it can be difficult to determine the initial outer shield coil turns because the boundary condition of a decrease of the PTE cannot be estimated without calculation. In this case, a practical method can be utilized to determine the boundary condition by comparing the inductance between the initial inner coil inductance and the iS inductance including the outer coil loop.

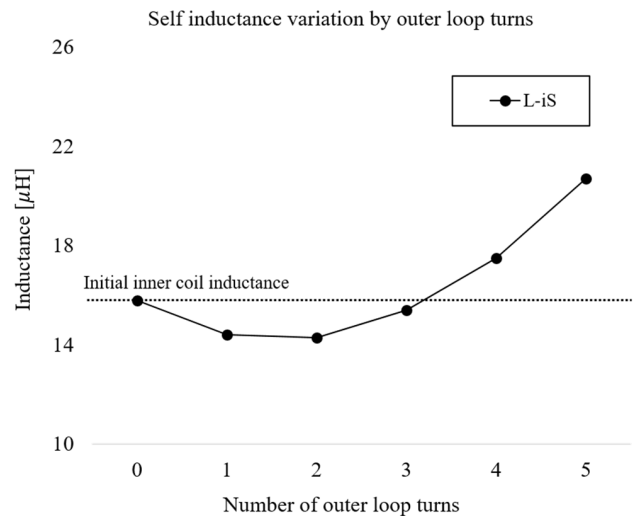


FIGURE 12. Self-inductance variation according to the number of outer shield coil turns.

Figure 12 shows the self-inductance variation of the iS coil according to the number of outer shield coil turns. When the outer shield coil is added to the inner shield coil, the inductance of the iS coil is changed according to (4). The iS inductance is decreased when the number of outer coil turns is less than four turns compared with the initial inner coil inductance having no outer coil loop. This can be a boundary condition of PTE enhancement by capacitance tuning.

The boundary condition is when the self-inductance of the outer coil loop $L_{out-self}$ and the mutual inductance between inner and outer coil M_{in-out} is equal. ($L_{out-self} = M_{in-out}$). Specifically, outer coil turns cause an increase of the iS inductance because of the increase of coil length. However, outer coil turns make negative mutual inductance with the inner coil loop as well. If $L_{out-self}$ and M_{in-out} are equal, the dual loop shield coil can be treated as a single loop having reduced inductance. As a result, the number of outer coil turns not over the boundary condition can contribute to increase the PTE by capacitance tuning. Based on these characteristics, the boundary condition of the number of outer coil turns without a PTE decrease can be estimated.

This method is only for estimating initial design criteria in terms of the practical design initiation strategy for preventing

a decrease of the PTE. In addition, this method is limited under the condition that the outer radius of the inner shield coil $r_{iSin-outer}$ and the inner radius of the outer shield coil $r_{iSout-inner}$ are identical. ($r_{iSin-outer} \cong r_{iSout-inner}$).

Capacitance tuning is performed to determine the capacitance ratio between the iX and iS coils. The generalized capacitance tuning method is given as (25) and (26). The increase of the capacitance ratio increases the current ratio, and hence the PTE will increase based on the increased quality factor. However, an excessive current ratio causes a decrease of SE because the shielding EMF will be higher than the leakage EMF. For this reason, the capacitance ratio is estimated in terms of the total magnetic field according to (17).

In case the target PTE cannot be achieved even though the capacitance is tuned to have a high ratio, the number of outer shield coil turns should be reduced. On the other hand, the number of outer shield coil turns should be increased in case the target SE cannot be achieved. In other words, the tradeoff between the SE and PTE is the key element of the capacitance tuning.

IV. EXPERIMENTAL VERIFICATION

A. COMMON SETTING CONDITION

The proposed shielding method is tested by simulation and experiment. Electromagnetic simulations are conducted through ANSYS Maxwell software. The subjects of the experiment are 1) w/o shield, 2) active shield, 3) previous reactive shield, and 4) proposed shield.

All experiments have been conducted with a symmetric WPT system and an asymmetrical WPT system, respectively. In addition, all experiments were conducted under alignment and misalignment conditions, respectively. The alignment condition is that all coils have a coaxial array. The misalignment condition is that the RX coil has a lateral displacement for the TX coil.

Ferrite and aluminum plates have been applied for all simulations and experiments for the symmetric and the asymmetric WPT systems. The depth of applied ferrite and aluminum plate is 4 mm and 1 mm, respectively. The coil of the WPT systems is designed with identical 4 mm diameter of copper wires. All EMF measurements have been conducted under the condition of transmitting 200 W load power. The load resistance has been set to 10 Ω, and the operating frequency is 85 kHz. The air gap between the TX and RX coils is 130 mm both in the case of symmetry and asymmetry. The PTE for all experiments has been calculated as the load power divided by the total supplied power.

Figure 13 shows the EMF measurement setup of the experimental verification. The EMF of all experiments has been measured by a magnetic field probe, NARDA Safety Test Solutions ELT-400, GmbH. EMF measurement points (MP_{*i*}) are set to left (MP₁), right (MP₂) top (MP₃), and bottom (MP₄) from the center of the WPT system. Each MP_{*i*} has three sub measurement points, MP_{*i*1}, MP_{*i*2}, and MP_{*i*3},



FIGURE 13. EMF Measurement setup.

and the total EMF of each experimental subject has been calculated as the average of four MP_{*i*}, as in (32). The SE of each shielding method is calculated using (33).

$$B_{MPi} = \frac{B_{MPi1} + B_{MPi2} + B_{MPi3}}{3} \quad (31)$$

$$B_{average} = \frac{B_{MP1} + B_{MP2} + B_{MP3} + B_{MP4}}{4} \quad (32)$$

$$SE = \left(1 - \frac{B_{average-w/ shield}}{B_{average-w/o shield}} \right) \times 100 \quad (33)$$

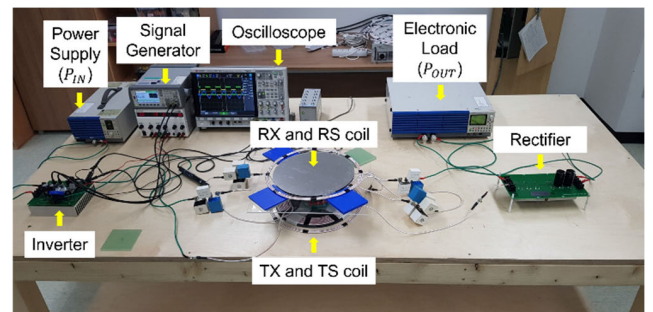


FIGURE 14. Experimental setup of symmetric WPT system.

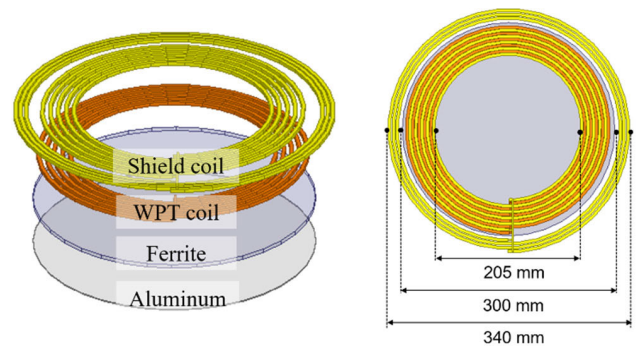


FIGURE 15. Coil geometry of proposed shield coil (Symmetric).

B. EXPERIMENTS FOR SYMMETRIC WPT SYSTEM

1) EXPERIMENTAL SETUP

Figure 14 shows the experimental setup of the symmetric WPT system. DC power supply supplies power (P_{IN}) to the inverter, and the inverter converts DC to AC. The transmitted AC power to the RX coil is converted again to DC through

the rectifier, and the converted DC power is transferred to the electronic load (P_{OUT}).

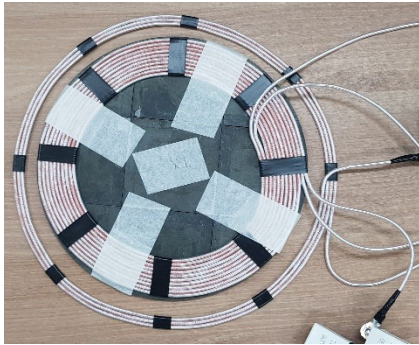


FIGURE 16. Fabricated coil for proposed shielding method (Symmetric).

Figure 15 shows the coil geometry of the proposed shielding method for the symmetric WPT system, and Figure 16 shows the fabricated coil. In the case of the symmetric WPT system, TX, RX, inner TS, and inner RS coils have identical coil radius. The inner diameters of TX, RX, inner TS, and inner RS are 205 mm. The diameters of ferrite and aluminum plate are identically 300 mm. The outer diameters of outer TS and RS are 340 mm.

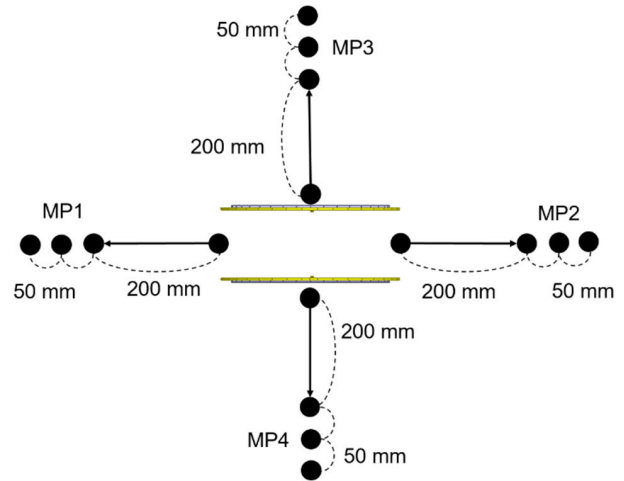
Figure 17(a) shows the MP_i of the aligned symmetric WPT system. Each sub measurement point in MP_i is at 200, 250, and 300 mm distance from the WPT system, respectively. Figure 17(b) shows the MP_i of the misaligned symmetric WPT system. The misalignment condition in the symmetric WPT system is that the RX coil has 50 mm lateral displacement for the TX coil. All measurement points are identical with the MP_i of the symmetric WPT system.

Table 1 presents the design parameters and Table 2 shows the electrical parameters for all experimental subjects of the symmetric WPT system. The current magnitude of the TX and RX coils is different according to the experimental subject. The load power of all experimental subjects is set at about 200W.

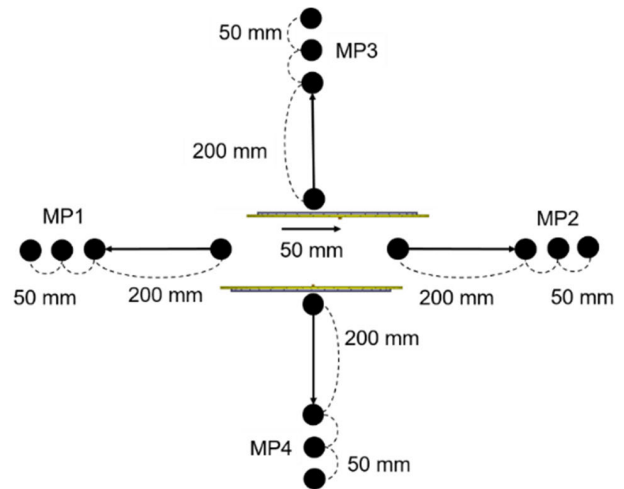
2) EXPERIMENTAL RESULTS

Figure 18 shows the simulation and experimental results of the transferred power to load for the symmetric WPT system in the alignment condition. All experimental subjects have about a 200 W load power condition. The simulations and experimental results of load power show less than a 5% difference. The experimentally measured load power of the case w/o shield was 206 W, and that of the proposed shielding method was 208 W. The load power of the active and previous reactive shield was 206 W and 203 W, respectively.

Figure 19 shows the simulation and experimental results of PTE for the symmetric WPT system in the alignment condition. The PTE of the case w/o shield was 82.6%, and that of the proposed shielding method was 84.7%. This shows a 2.1% PTE increase compared with the case w/o shield. The PTE of the dependent active shield was 73.7%, and this is an



(a) Measurement points of aligned symmetric WPT system



(b) Measurement points of misaligned symmetric WPT system

FIGURE 17. Measurement points of symmetric WPT system.

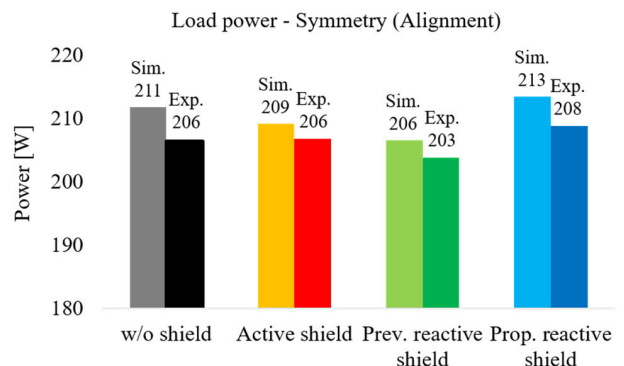


FIGURE 18. Simulation and experimental results of load power for symmetric WPT system (Alignment).

8.9% PTE decrease compared with the case w/o shield. The PTE of the previous reactive shield was 75.3%, and this is a 7.3% PTE decrease.

TABLE 1. Design parameters of symmetric WPT system.

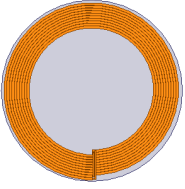
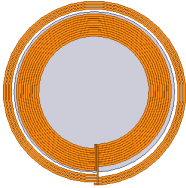
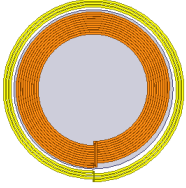
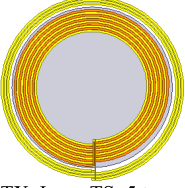
	w/o shield	Active shield	Previous reactive shield	Proposed shield
Coil geometry	 TX, RX: 10 turns	 Inner TX, RX: 10 turns Outer TX, RX: 3 turns	 TX, RX: 10 turns TS, RS: 3 turns	 TX, Inner TS: 5 turns RX, Inner RS: 5 turns Outer TS, RS: 3 turns
$L_{TX} [\mu T]$	60.4	57.6	60.4	15.9
$L_{RX} [\mu T]$	59.2	56.8	59.2	15.8
$L_{TS} [\mu T]$	-	-	7.8	19.1
$L_{RS} [\mu T]$	-	-	7.8	20.4
$C_{TX} [nF]$	55	59.4	61.7	86.3
$C_{RX} [nF]$	58.4	61.5	61.6	68.5
$C_{TS} [nF]$	-	-	2.4 [μF]	148.2
$C_{RS} [nF]$	-	-	2.4 [μF]	148.2

TABLE 2. Electrical parameters of symmetric WPT system.

Subject	w/o shield		Active shield		Previous reactive shield		Proposed shield	
	Align	Misalign	Align	Misalign	Align	Misalign	Align	Misalign
Coil array								
$I_{TX} \angle \phi_{TX} [A \angle ^\circ]$	17.5 \angle 0°	22 \angle 0°	25.2 \angle 0°	32 \angle 0°	26 \angle 0°	33 \angle 0°	12.8 \angle 0°	13.6 \angle 0°
$I_{RX} \angle \phi_{RX} [A \angle ^\circ]$	8.2 \angle 86°	8.3 \angle 87°	8.3 \angle 91°	8.3 \angle 91°	8.3 \angle 89°	8.4 \angle 92°	15.3 \angle 109°	15.5 \angle 111°
$I_{TS} \angle \phi_{TS} [A \angle ^\circ]$	-	-	-	-	23 \angle -172°	29 \angle -178°	23 \angle 11°	29 \angle 23°
$I_{RS} \angle \phi_{RS} [A \angle ^\circ]$	-	-	-	-	7.6 \angle -123°	8.1 \angle -127°	23 \angle 95°	25 \angle 104°
$P_L [W]$	206.3	207.4	206.7	201.6	203.7	206.5	208.8	207.6

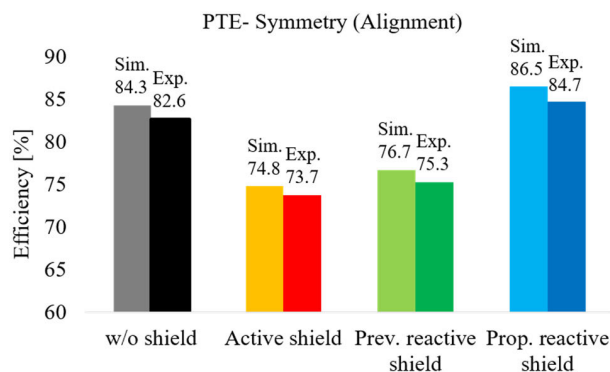


FIGURE 19. Simulation and experimental results of PTE for symmetric WPT system (Alignment).

Figure 20 shows the simulation and experimental results of the SE for the symmetric WPT system in the alignment condition. The average SE of the dependent active shield was 49.1%, and that of the previous reactive shield was 51.8%. The average SE of the proposed shielding method was 55.5%, and the SE difference with the active shield and previous reactive shield is 6.4% and 3.7%, respectively.

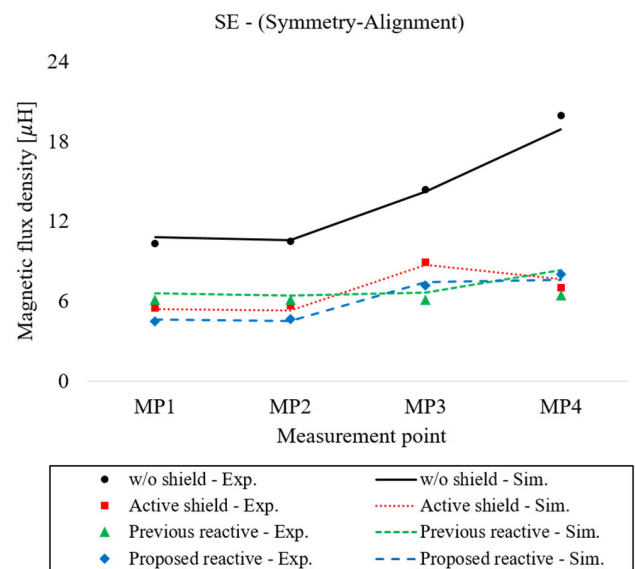


FIGURE 20. Simulation and experimental results of SE for symmetric WPT system (Alignment).

Figure 21 shows the simulation and experimental results of the transferred power to load for the symmetric WPT system

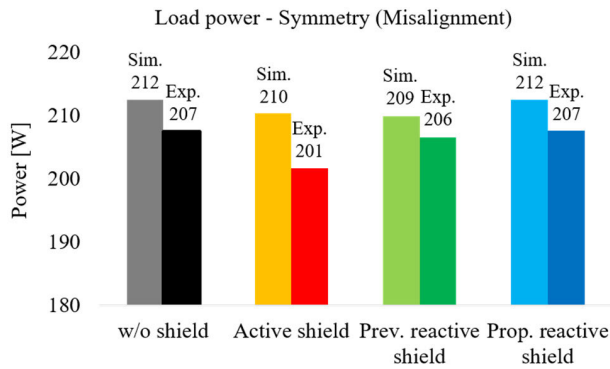


FIGURE 21. Simulation and experimental results of load power for symmetric WPT system (Misalignment).

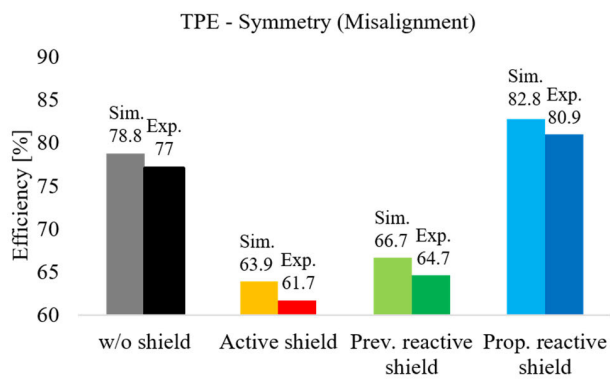


FIGURE 22. Simulation and experimental results of PTE for symmetric WPT system (Misalignment).

in the misalignment condition. Likewise, all experimental subjects have about a 200 W load power condition and under a 5% difference with the simulation results. The experimentally measured load power of the case w/o shield and the proposed shielding method was identically 207 W. The load power of active and previous reactive shield was 201 W and 206 W, respectively.

Figure 22 shows the simulation and experimental results of the PTE for the symmetric WPT system in the misalignment condition. In the case of w/o shields, the PTE was 77%. The PTE of the proposed shielding method was 80.9%, and this result is a 3.9% increased PTE compared with the case w/o shields. The PTE of the dependent active shield was 61.7%, and this result is a 15.3% PTE decrease compared with the case w/o shield. The PTE of the previous reactive shield was 64.7%, and this result is a 12.3% PTE decrease compared with the case w/o shield.

Figure 23 shows the simulation and experimental results of SE for the symmetric WPT system in the misalignment condition. The SE of all shielding methods decreased in the misalignment condition. The average SE of the dependent active shield was 41%, and that of the previous reactive shield was 46.5%. The average SE of the proposed shield was 53%, and the SE difference with the active shield and previous reactive shield is 12% and 6.5%, respectively.

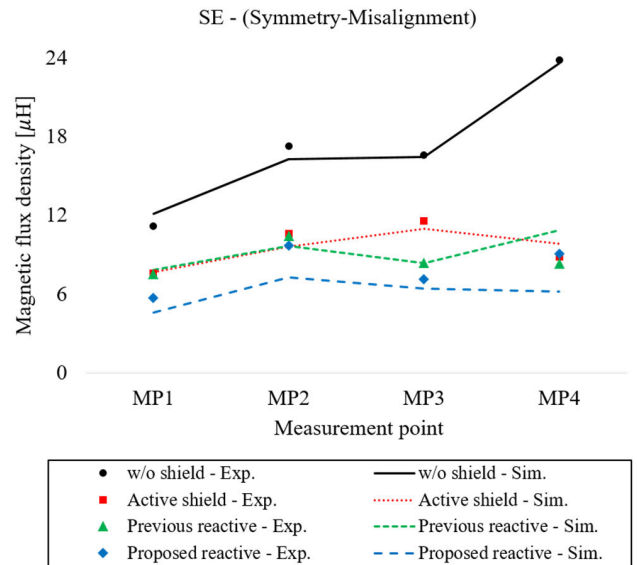


FIGURE 23. Simulation and experimental results of SE for symmetric WPT system (Misalignment).

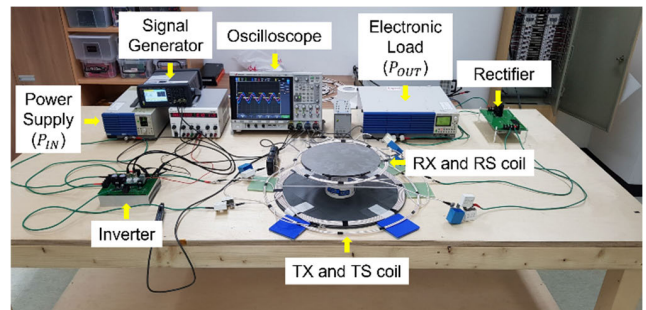


FIGURE 24. Experimental setup of asymmetric WPT system.

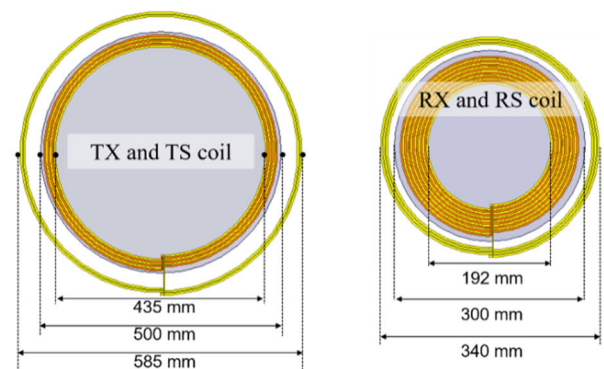


FIGURE 25. Coil geometry of proposed shield coil (Asymmetric).

C. EXPERIMENTS FOR ASYMMETRIC WPT SYSTEM

1) EXPERIMENTAL SETUP

Figure 24 shows the experimental setup of the asymmetric WPT system. The setup of the asymmetric WPT system is identical to that of the symmetric WPT system except for the coils.

TABLE 3. Design parameters of asymmetric WPT system.

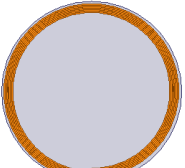
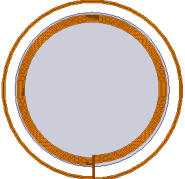
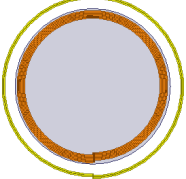
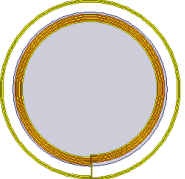
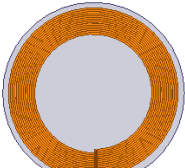
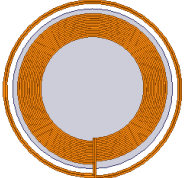
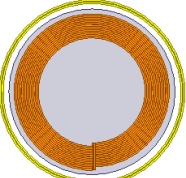
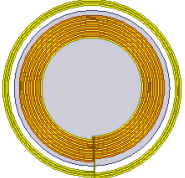
	w/o shield	Active shield	Previous reactive shield	Proposed shield
Coil geometry (TX side)	 TX: 6 turns	 Inner TX: 6 turns Outer TX: 2 turns	 TX: 6 turns TS: 2 turns	 TX, Inner TS: 3 turns Outer TS: 2 turns
Coil geometry (RX side)	 RX: 14 turns	 Inner RX: 14 turns Outer RX: 3 turns	 RX: 14 turns RS: 3 turns	 RX, Inner RS: 7 turns Outer RS: 3 turns
L_{TX} [μT]	50.9	50.8	50.8	13.3
L_{RX} [μT]	119.3	113.9	119.3	30.7
L_{TS} [μT]	-	-	8	16.9
L_{RS} [μT]	-	-	9.2	32.2
C_{TX} [nF]	65.1	68.9	74.8	106
C_{RX} [nF]	29.5	30.3	30.5	29.55
C_{TS} [nF]	-	-	990	144.7
C_{RS} [nF]	-	-	1.8 [μF]	86.5

TABLE 4. Electrical parameters of asymmetric WPT system.

Subject	w/o shield		Active shield		Previous reactive shield		Proposed shield	
	Align	Misalign	Align	Misalign	Align	Misalign	Align	Misalign
$I_{TX} \angle \phi_{TX}$ [$A \angle ^\circ$]	18.2 \angle 0°	19 \angle 0°	29 \angle 0°	30 \angle 0°	27 \angle 0°	30 \angle 0°	12.8 \angle 0°	13.6 \angle 0°
$I_{RX} \angle \phi_{RX}$ [$A \angle ^\circ$]	8.3 \angle 94°	8.3 \angle 94°	8.3 \angle 89°	8.3 \angle 88°	8.2 \angle 95°	8.2 \angle 96°	15.3 \angle 109°	15.5 \angle 111°
$I_{TS} \angle \phi_{TS}$ [$A \angle ^\circ$]	-	-	-	-	32 \angle -175°	34 \angle -172°	23 \angle 11°	29 \angle 23°
$I_{RS} \angle \phi_{RS}$ [$A \angle ^\circ$]	-	-	-	-	13.5 \angle -126°	10.3 \angle -121°	23 \angle 95°	25 \angle 104°
P_L [W]	201.1	204.2	202.7	204.3	201.6	201.6	208.8	207.6

Table 3 presents the design parameters, and Table 4 gives the electrical parameters for all experimental subjects of the asymmetric WPT system. The load power of all experimental subjects is similarly about 200W as in the case of the symmetric WPT system.

Figure 25 and Figure 26 are the coil geometry and the fabricated TX and RX coils of the proposed shielding method for the asymmetrical WPT system. The radius of the TX coil in the asymmetrical WPT system is larger than that of the RX coil. The TX and the inner TS have identical 435 mm inner diameter. The diameter of the ferrite and aluminum plate applied to the TX coil is identically 500 mm. The outer diameter of the outer TS is 585 mm. The RX and inner RS have identical 192 mm inner diameter. The outer diameter of the outer RS is 340 mm. The diameter of the ferrite and aluminum plate applied to the RX coil is identically 300 mm.

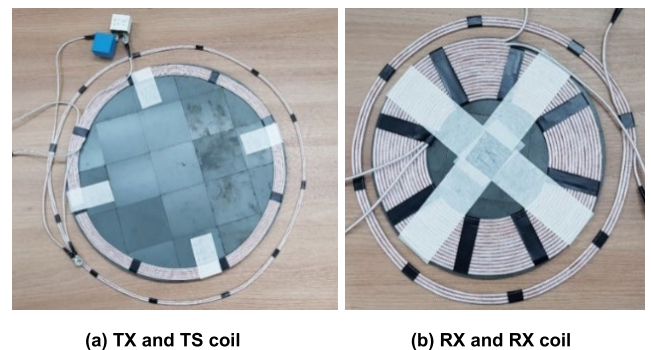
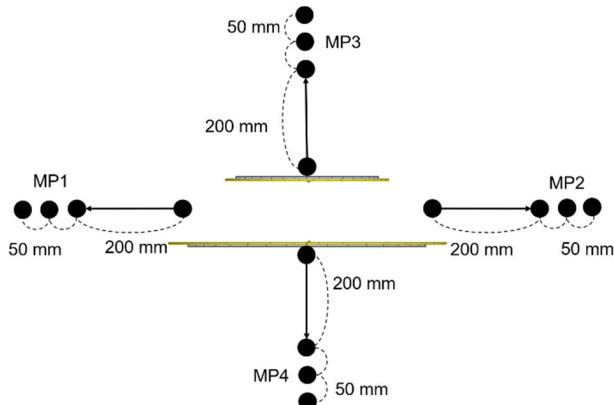
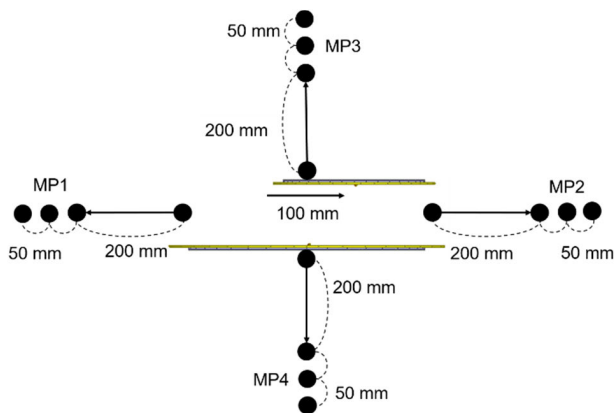


FIGURE 26. Fabricated coil for proposed shield (Asymmetric).

Figure 27(a) shows the MPi of the aligned asymmetric WPT system. Each sub measurement point in MP1 and MP2 has 200, 250, and 300 mm distance from the TX coil, respectively. MP3 and MP4 are identical to the case of the



(a) Measurement points of aligned asymmetric WPT system



(b) Measurement points of misaligned asymmetric WPT system

FIGURE 27. Measurement points of asymmetric WPT system.

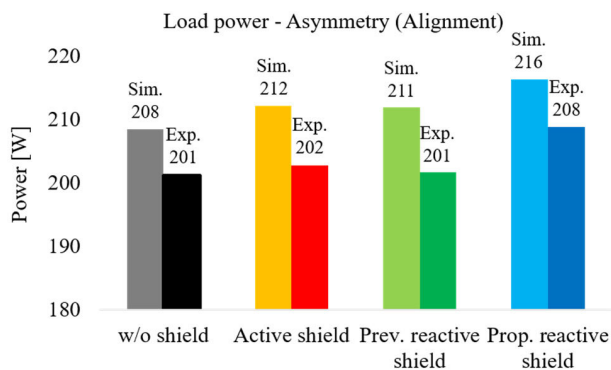


FIGURE 28. Simulation and experimental results of load power for asymmetric WPT system (Alignment).

symmetric WPT system. Figure 27(b) shows the MP_i of the misaligned asymmetric WPT system. The misalignment condition in the asymmetric WPT system is that the RX coil has 100 mm lateral displacement for the TX coil.

2) EXPERIMENTAL RESULTS

Figure 28 shows the simulation and experimental results of the transferred power to load for the asymmetric WPT system

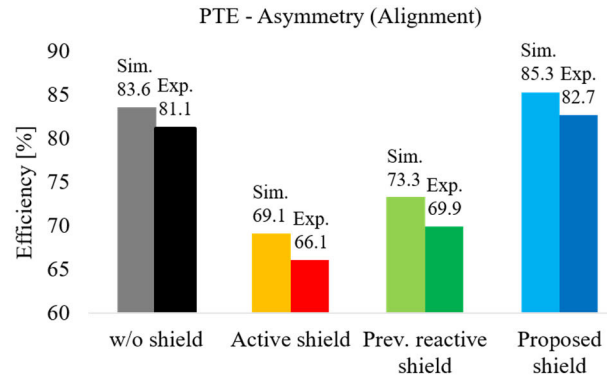


FIGURE 29. Simulation and experimental results of PTE for asymmetric WPT system (Alignment).

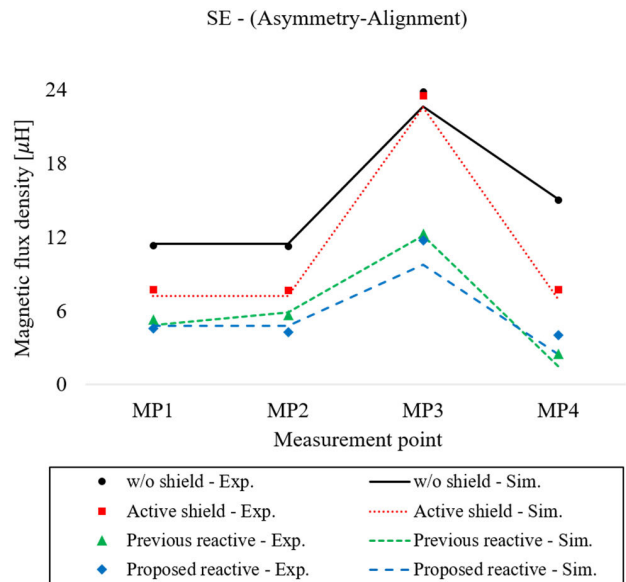


FIGURE 30. Simulation and experimental results of SE for asymmetric WPT system (Alignment).

in the alignment condition. The experimentally measured load power of the case w/o shield and the proposed shielding method were 201 W and 208 W, respectively. The load power of the active and previous reactive shield was 202 W and 201 W, respectively.

Figure 29 shows the simulation and experimental results of PTE for the asymmetric WPT system in the alignment condition. In the case of w/o shield, the PTE was 81.1%. The PTE of the proposed shielding method was 82.7%, and this result is a 1.6% increased PTE compared with the case w/o shield. The PTE of the dependent active shield was 66.1%, and this result is a 15% decreased PTE compared with the case w/o shield. The PTE of the previous reactive shield was 69.9%, and this result is a 11.2% PTE decrease.

Figure 30 shows the simulation and experimental results of SE for the asymmetric WPT system in the alignment condition. The average SE of the dependent active shield was 28.1% and the previous reactive shield was 58.4%. The average SE of the proposed shield was 61.3%, and the SE

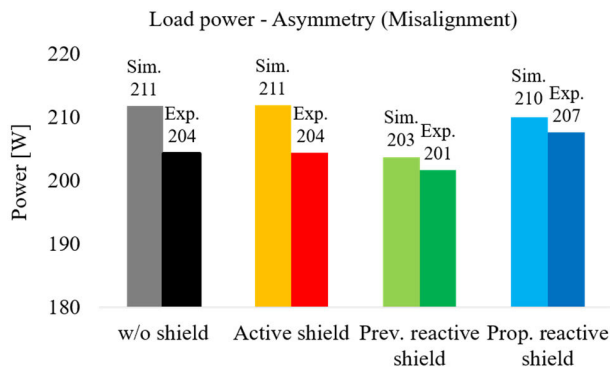


FIGURE 31. Simulation and experimental results of load power for asymmetric WPT system (Misalignment).

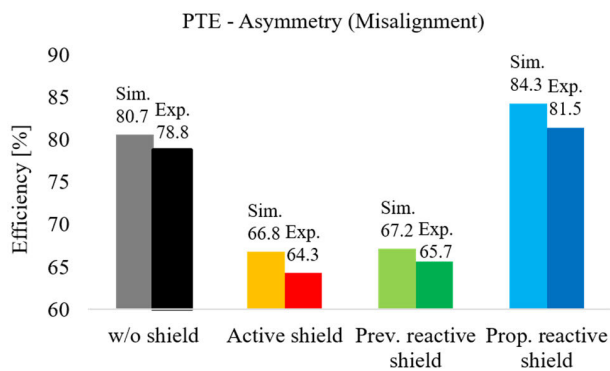


FIGURE 32. Simulation and experimental results of PTE for asymmetric WPT system (Misalignment).

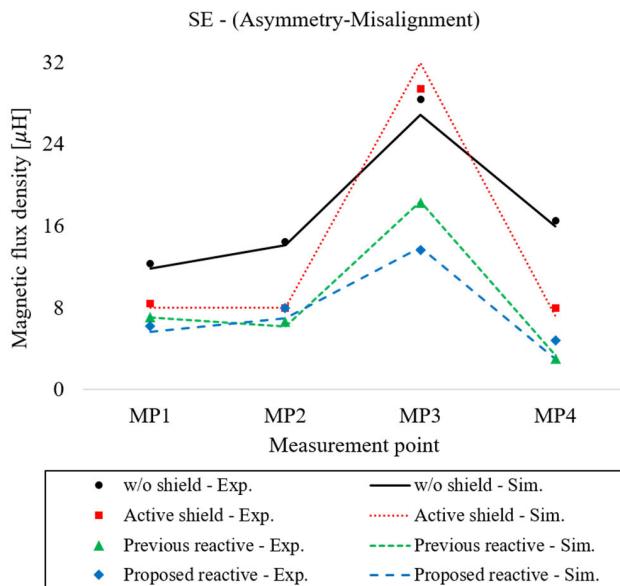


FIGURE 33. Simulation and experimental results of SE for asymmetric WPT system (Misalignment).

difference with the active shield and previous reactive shield is 33.2% and 2.9%, respectively.

Figure 31 shows the simulation and experimental results of the transferred power to load for the asymmetric WPT system

in misalignment condition. The experimentally measured load power of the case w/o shield and the proposed shielding method was respectively 204 W and 207 W. The load power of the active and previous reactive shield was 204 W and 201 W.

Figure 32 shows the simulation and experimental results of PTE for the symmetric WPT system in the misalignment condition. In the case of the w/o shield, the PTE was 78.8%. The PTE of the proposed shielding method was 81.5%, and this result is a 2.7% increased PTE compared with the case w/o shield. The PTE of the dependent active shield was 64.3%, and this result is the 14.5% PTE decrease compared with the case w/o shield. The PTE of the previous reactive shield was 65.7%, and this result is a 13.1% PTE decrease.

Figure 33 shows the simulation and experimental results of SE for the asymmetric WPT system in the misalignment condition. The average SE of the dependent active shield was 31.1%, and that of the previous reactive shield was 53.3%. The average SE of the proposed shield was 54.1%, and the SE difference with the active shield and the previous reactive shield was 23% and 0.8%, respectively.

V. CONCLUSION

In this paper, a dual loop reactive shield application of a WPT system for leakage EMF reduction and PTE enhancement has been proposed. The proposed shield provides an increase of PTE with SE based on simultaneous in phase and out of phase magnetic field generation. A method of boosting the quality factor based on current ratio control by capacitance tuning has been proposed. In addition, the proposed method is beneficial for maintaining the PTE in a misalignment condition. The proposed method has been verified for symmetric and asymmetric WPT systems including a misalignment condition. The experimental results of the proposed method with the symmetric WPT system showed a 2.1% PTE increase with 55.5% SE in an alignment condition, and a 3.9% PTE increase with 53% SE in a misalignment condition. In addition, the experimental results of the proposed method with the asymmetric WPT system revealed a 1.6% PTE increase with 61.3% SE in an alignment condition, and a 2.7% PTE increase with 54.1% SE in a misalignment condition.

ACKNOWLEDGMENT

The authors would like to acknowledge the technical support from ANSYS Korea.

REFERENCES

- [1] A. Kurs, A. Karalis, R. Moffatt, J. D. Joannopoulos, P. Fisher, and M. Soljačić, "Wireless power transfer via strongly coupled magnetic resonances," *Science*, vol. 317, no. 5834, pp. 83–86, 2007, doi: 10.1126/science.1143254.
- [2] S. Jeong, "Smartwatch strap wireless power transfer system with flexible PCB coil and shielding material," *IEEE Trans. Ind. Electron.*, vol. 66, no. 5, pp. 4054–4064, May 2019, doi: 10.1109/TIE.2018.2860534.
- [3] J.-Q. Zhu, Y.-L. Ban, Y. Zhang, Z. Yan, R.-M. Xu, and C. C. Mi, "Three-coil wireless charging system for metal-cover smartphone applications," *IEEE Trans. Power Electron.*, vol. 35, no. 5, pp. 4847–4858, May 2020, doi: 10.1109/TPEL.2019.2944845.

- [4] A. B. Junaid, Y. Lee, and Y. Kim, "Design and implementation of autonomous wireless charging station for rotary-wing UAVs," *Aerosp. Sci. Technol.*, vol. 54, pp. 253–266, Jul. 2016, doi: [10.1016/j.ast.2016.04.023](https://doi.org/10.1016/j.ast.2016.04.023).
- [5] M. Lu, M. Bagheri, A. P. James, and T. Phung, "Wireless charging techniques for UAVs: A review, reconceptualization, and extension," *IEEE Access*, vol. 6, pp. 29865–29884, 2018, doi: [10.1109/ACCESS.2018.2841376](https://doi.org/10.1109/ACCESS.2018.2841376).
- [6] J. Zhou, B. Zhang, W. Xiao, D. Qiu, and Y. Chen, "Nonlinear parity-time-symmetric model for constant efficiency wireless power transfer: Application to a drone-in-flight wireless charging platform," *IEEE Trans. Ind. Electron.*, vol. 66, no. 5, pp. 4097–4107, May 2019, doi: [10.1109/TIE.2018.2864515](https://doi.org/10.1109/TIE.2018.2864515).
- [7] *IEEE Standard for Safety Levels with Respect to Human Exposure to Radio Frequency Electromagnetic Fields, 3 kHz to 300 GHz*, IEEE Standard C95.1, Edition, Apr. 1999, pp. 1–83.
- [8] ICNIRP, "Guidelines for limiting exposure to time-varying electric and magnetic fields (1 Hz to 100 kHz)," *Health Phys.*, vol. 99, no. 6, pp. 818–836, 2010.
- [9] J. Kim, J. Kim, S. Kong, H. Kim, I.-S. Suh, N. P. Suh, and D.-H. Cho, "Coil design and shielding methods for a magnetic resonant wireless power transfer system," *Proc. IEEE*, vol. 101, no. 6, pp. 1332–1342, Jun. 2013, doi: [10.1109/JPROC.2013.2247551](https://doi.org/10.1109/JPROC.2013.2247551).
- [10] Y. Yashima, H. Omori, T. Morizane, N. Kimura, and M. Nakaoka, "Leakage magnetic field reduction from wireless power transfer system embedding new eddy current-based shielding method," in *Proc. Int. Conf. Electr. Drives Power Electron. (EDPE)*, Sep. 2015, pp. 241–245, doi: [10.1109/EDPE.2015.7325300](https://doi.org/10.1109/EDPE.2015.7325300).
- [11] J. Shin, S. Shin, Y. Kim, S. Ahn, S. Lee, G. Jung, S.-J. Jeon, and D.-H. Cho, "Design and implementation of shaped magnetic-resonance-based wireless power transfer system for roadway-powered moving electric vehicles," *IEEE Trans. Ind. Electron.*, vol. 61, no. 3, pp. 1179–1192, Apr. 2014, doi: [10.1109/TIE.2013.2258294](https://doi.org/10.1109/TIE.2013.2258294).
- [12] S. Y. Choi, B. W. Gu, S. W. Lee, W. Y. Lee, J. Huh, and C. T. Rim, "Generalized active EMF cancel methods for wireless electric vehicles," *IEEE Trans. Power Electron.*, vol. 29, no. 11, pp. 5770–5783, Nov. 2014, doi: [10.1109/TPEL.2013.2295094](https://doi.org/10.1109/TPEL.2013.2295094).
- [13] S. Cruciani, T. Campi, F. Maradei, and M. Feliziani, "Active shielding design for wireless power transfer systems," *IEEE Trans. Electromagn. Compat.*, vol. 61, no. 6, pp. 1953–1960, Dec. 2019, doi: [10.1109/TEMC.2019.2942264](https://doi.org/10.1109/TEMC.2019.2942264).
- [14] J. Kim, J. Ahn, S. Huh, K. Kim, and S. Ahn, "A coil design and control method of independent active shielding system for leakage magnetic field reduction of wireless UAV charger," *IEICE Trans. Commun.*, vol. 103, no. 9, pp. 889–898, Sep. 2020, doi: [10.1587/transcom.2019MCI0001](https://doi.org/10.1587/transcom.2019MCI0001).
- [15] S. Kim, H.-H. Park, J. Kim, J. Kim, and S. Ahn, "Design and analysis of a resonant reactive shield for a wireless power electric vehicle," *IEEE Trans. Microw. Theory Techn.*, vol. 62, no. 4, pp. 1057–1066, Apr. 2014, doi: [10.1109/TMTT.2014.2305404](https://doi.org/10.1109/TMTT.2014.2305404).
- [16] H. Moon, S. Kim, H. H. Park, and S. Ahn, "Design of a resonant reactive shield with double coils and a phase shifter for wireless charging of electric vehicles," *IEEE Trans. Magn.*, vol. 51, no. 3, Mar. 2015, Art. no. 8700104, doi: [10.1109/TMAG.2014.2360701](https://doi.org/10.1109/TMAG.2014.2360701).
- [17] J. Park, D. Kim, K. Hwang, H. H. Park, S. I. Kwak, J. H. Kwon, and S. Ahn, "A resonant reactive shielding for planar wireless power transfer system in smartphone application," *IEEE Trans. Electromagn. Compat.*, vol. 59, no. 2, pp. 695–703, Apr. 2017, doi: [10.1109/TEMC.2016.2636863](https://doi.org/10.1109/TEMC.2016.2636863).
- [18] S. R. Khan, S. K. Pavuluri, and M. P. Y. Desmulliez, "Accurate modeling of coil inductance for near-field wireless power transfer," *IEEE Trans. Microw. Theory Techn.*, vol. 66, no. 9, pp. 4158–4169, Sep. 2018, doi: [10.1109/TMTT.2018.2854190](https://doi.org/10.1109/TMTT.2018.2854190).
- [19] C.-J. Chen, T.-H. Chu, C.-L. Lin, and Z.-C. Jou, "A study of loosely coupled coils for wireless power transfer," *IEEE Trans. Circuits Syst. II, Exp. Briefs*, vol. 57, no. 7, pp. 536–540, Jul. 2010, doi: [10.1109/TCSII.2010.2048403](https://doi.org/10.1109/TCSII.2010.2048403).
- [20] D. Ahn and S. Hong, "A study on magnetic field repeater in wireless power transfer," *IEEE Trans. Ind. Electron.*, vol. 60, no. 1, pp. 360–371, Jan. 2013, doi: [10.1109/TIE.2012.2188254](https://doi.org/10.1109/TIE.2012.2188254).
- [21] D. Ahn and S. Hong, "A transmitter or a receiver consisting of two strongly coupled resonators for enhanced resonant coupling in wireless power transfer," *IEEE Trans. Ind. Electron.*, vol. 61, no. 3, pp. 1193–1203, Mar. 2014, doi: [10.1109/TIE.2013.2257151](https://doi.org/10.1109/TIE.2013.2257151).
- [22] K. Lee and S. H. Chae, "Power transfer efficiency analysis of intermediate-resonator for wireless power transfer," *IEEE Trans. Power Electron.*, vol. 33, no. 3, pp. 2484–2493, Mar. 2018, doi: [10.1109/TPEL.2017.2698638](https://doi.org/10.1109/TPEL.2017.2698638).
- [23] D. H. Tran, V. B. Vu, and W. Choi, "Design of a high-efficiency wireless power transfer system with intermediate coils for the on-board chargers of electric vehicles," *IEEE Trans. Power Electron.*, vol. 33, no. 1, pp. 175–187, Jan. 2018, doi: [10.1109/TPEL.2017.2662067](https://doi.org/10.1109/TPEL.2017.2662067).
- [24] A. P. Sample, D. A. Meyer, and J. R. Smith, "Analysis, experimental results, and range adaptation of magnetically coupled resonators for wireless power transfer," *IEEE Trans. Ind. Electron.*, vol. 58, no. 2, pp. 544–554, Feb. 2011, doi: [10.1109/TIE.2010.2046002](https://doi.org/10.1109/TIE.2010.2046002).



JEDOK KIM received the M.S. degree in industrial engineering from Hanyang University, Seoul, South Korea. He is currently pursuing the Ph.D. degree with KAIST. His research interests include safety enhancement of wireless power transfer systems, leakage magnetic field reduction, and foreign object detection in wireless power transfer systems for greater human safety.



SEUNGYOUNG AHN (Senior Member, IEEE) received the B.S., M.S., and Ph.D. degrees in electrical engineering from Korea Advanced Institute of Science and Technology (KAIST), Daejeon, South Korea, in 1998, 2000, and 2005, respectively. From 2005 to 2009, he was a Senior Engineer with Samsung Electronics, Suwon, South Korea, where he was in charge of high-speed board design for laptop computer systems. He is currently an Associate Professor

with The Cho Chun Shik Graduate School of Green Transportation, KAIST. His research interests include wireless power transfer system design and electromagnetic compatibility design for electric vehicles and high-performance digital systems.

...